3rd URSI AT-AP-RASC, Gran Canaria, 29 May – 3 June 2022

Alternative Definitions of the Field Anisotropy in a Reverberation Chamber

Qian Xu (1), Xueqi Shen(2), Peng Peng(3), Tian Hong Loh* (4) and Yi Huang(5)
(1) Nanjing University of Aeronautics and Astronautics, Nanjing 211106, China, https://www.nuaa.edu.cn/
(2) Nanjing Rongce Testing Technology Ltd., Nanjing 211112, China, http://en.emcdir.cn/
(3) Ford Motor Research and Engineering (Nanjing) Co., Ltd., Nanjing 211100, China, https://www.ford.com/
(4) National Physical Laboratory, Teddington, Middlesex TW11 0LW, United Kingdom, https://www.npl.co.uk/
(5) The University of Liverpool, Liverpool L79 3BX, United Kingdom, https://www.liverpool.ac.uk/

Abstract

In this paper, we propose alternative definitions on the statistical field anisotropy in a reverberation chamber. The proposed definitions are more direct and intuitive compared to the conventional definitions in the IEC 61000-4-21 standard. The equivalency between the proposed definitions and the conventional definitions is presented. The probability density and cumulative distribution functions of the proposed anisotropy coefficient are derived. Measurement demonstrations are also given.

1. Introduction

The anisotropy coefficient in a reverberation chamber (RC) quantifies the statistical imbalance between different polarizations of the E-fields (or H-fields) which is one of the key figures of merit. A common approach to characterize the RC anisotropy coefficient is based on polarization balance by acquiring the electric field or received power for each of three orthogonal polarizations of an electric-field probe or antenna at eight different locations inside the RC that form the edge of the chamber's working volume. The definition of the anisotropy has been detailed in the IEC 61000-4-21 standard [1].

$$A_{ij} \overset{\text{def}}{=} \frac{|E_i|^2 - |E_j|^2}{|E_i|^2 + |E_j|^2}, \quad (i,j = x,y,z; i \neq j) \quad (1)$$

$$A \overset{\text{def}}{=} \sqrt{\frac{A_{xy}^2 + A_{yz}^2 + A_{zx}^2}{3}} \quad (2)$$

where A_{ij} is the planar anisotropy coefficient, $|E_i|^2, (i = x,y,z)$ represents the squared E-field (received power) sample measured in an RC and A represents the total anisotropy coefficient. One supposes that the received power samples follow an exponential distribution

$$p_{E_i}(x_i) = \frac{1}{\mu_i} e^{-\frac{x_i}{\mu_i}}, \quad i = 1, 2 \text{ or } 3 \quad (3)$$

where x_1, x_2 and x_3 represent the received power in different polarizations ($|E_x|^2$, $|E_y|^2$ and $|E_z|^2$), the mean and standard deviations are both μ_i. The probability density function (PDF) and the cumulative distribution function (CDF) of A_{ij} have been detailed in [1-9] which are

$$p_{A_{ij}}(x) = \frac{2\sigma_r}{[\sigma_r + 1 + (\sigma_r - 1)x]}, \quad -1 \leq x \leq 1 \quad (4)$$

$$F_{A_{ij}}(x) = \frac{(1+x)\sigma_r}{[\sigma_r + 1 + (\sigma_r - 1)x]}, \quad -1 \leq x \leq 1 \quad (5)$$

where $\sigma_r = \mu_j/\mu_i$. The mean and the standard deviation of A_{ij} are [1, 2]

$$\mu_{A_{ij}} = \frac{1 + 2\sigma_r \ln\sigma_r - \sigma_r^2}{(\sigma_r - 1)^2} \quad (6)$$

$$\sigma_{A_{ij}} = \frac{2\sqrt{\sigma_r - (2 + \ln^2\sigma_r)\sigma_r^2 + \sigma_r^3}}{(\sigma_r - 1)^2} \quad (7)$$

The beauty of definition in (1) is: when $\sigma_r = 1$, $F_{A_{ij}}(x)$ is a linear function. However, the relationship between $\mu_{A_{ij}}$ and σ_r in (6) is a transcendental function and not intuitive, and it is not easy to identify σ_r from measured $\mu_{A_{ij}}$ at first glance.

2. Proposed Definitions

To construct a direct link between the mean value of the anisotropy and the ratio σ_r, we propose an alternative anisotropy coefficient random variable which is defined as

$$A'_{ij} \overset{\text{def}}{=} 10\log_{10}\frac{|E_i|^2}{|E_j|^2}, \quad (i,j = x,y,z; i \neq j) \quad (8)$$

which is the difference of the received power samples in dB form. By applying the principles of transformed variables, one could find the PDF and the CDF of A'_{ij} as

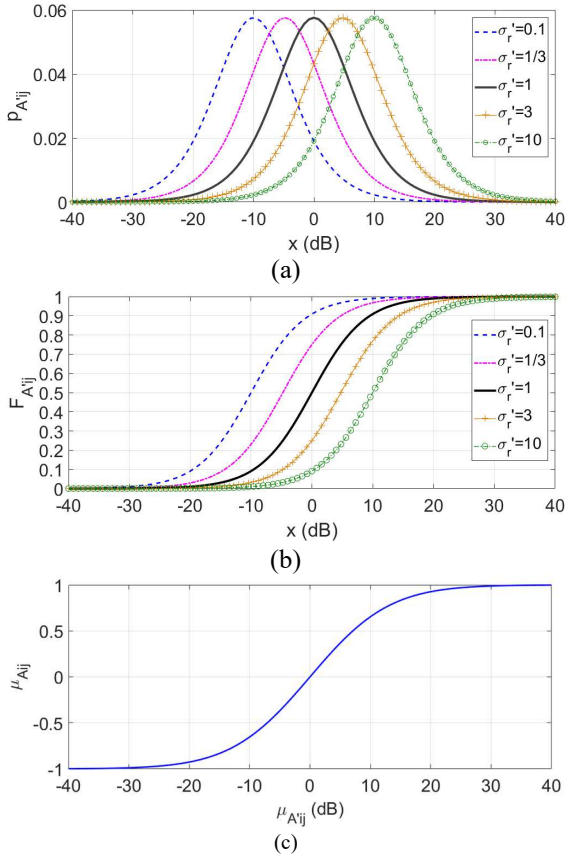

Figure 1. (a) PDF plots of A'_{ij}, (b) CDF plots of A'_{ij}, (c) the equivalency between $\mu_{A'_{ij}}$ and $\mu_{A_{ij}}$.

$$p_{A'_{ij}}(x) = \frac{10^{\frac{x}{10}-1}\sigma'_r \ln(10)}{(\sigma'_r + 10^{x/10})^2}, \qquad -\infty \le x \le \infty \quad (9)$$

$$F_{A'_{ij}}(x) = \frac{10^{x/10}}{\sigma'_r + 10^{x/10}}, \qquad -\infty \le x \le \infty \quad (10)$$

where $\sigma'_r = \mu_i/\mu_j = \sigma_r^{-1}$. The mean and the standard deviation of A'_{ij} are derived as

$$\mu_{A'_{ij}} = 10\log_{10}\sigma'_r \quad (11)$$

$$\sigma_{A'_{ij}} = \frac{10\pi}{\sqrt{3}\ln 10} \approx 7.877 \quad (12)$$

Interestingly, the mean value of A'_{ij} is directly the dB form of σ'_r and the standard deviation $\sigma_{A'_{ij}}$ is a constant. Typical plots of PDFs and CDFs with different are illustrated in Figure 1(a) and 1(b), the equivalency between $\mu_{A'_{ij}}$ and $\mu_{A_{ij}}$ is given in Figure 1(c). For the mean and standard deviation of the mean value from finite samples N ($\langle A_{ij}\rangle_N$ and $\langle A'_{ij}\rangle_N$), the results are derived as

$$\mu_{\langle A_{ij}\rangle_N} = \frac{1 + 2\sigma_r \ln\sigma_r - \sigma_r^2}{(\sigma_r - 1)^2} \quad (13)$$

$$\sigma_{\langle A_{ij}\rangle_N} = \frac{2}{\sqrt{N}} \frac{\sqrt{\sigma_r - (2 + \ln^2\sigma_r)\sigma_r^2 + \sigma_r^3}}{(\sigma_r - 1)^2} \quad (14)$$

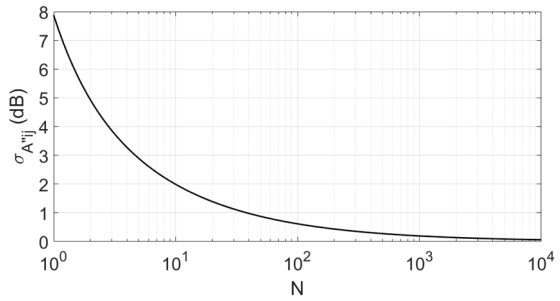

Figure 2. Plot of $\sigma_{A''_{ij}}$ with different independent sample number N.

$$\mu_{\langle A'_{ij}\rangle_N} = 10\log_{10}\sigma'_r \quad (15)$$

$$\sigma_{A'_{ij}} = \frac{1}{\sqrt{N}} \frac{10\pi}{\sqrt{3}\ln 10} \quad (16)$$

As can be seen, $\mu_{\langle A_{ij}\rangle_N}$ and $\mu_{\langle A'_{ij}\rangle_N}$ are both unbiased and the standard deviations decay with a speed of $1/\sqrt{N}$.
Another possible definition is to find the ratio of the mean values between $|E_i|^2$ and $|E_j|^2$

$$A''_{ij} \overset{\text{def}}{=} 10\log_{10} \frac{\langle |E_i|^2 \rangle_N}{\langle |E_j|^2 \rangle_N}, \qquad (i, j = x, y, z; i \ne j) \quad (17)$$

This random variable has been well investigated in many RC applications when the ratio of two variables is involved [10] (e.g. antenna efficiency measurement, shielding effectiveness), and the PDF of A''_{ij} can be derived as

$$p_{A''_{ij}}(x) = \frac{\Gamma(2N)\ln(10)10^{Nx/10-1}\sigma_r'^N}{\Gamma^2(N)(\sigma'_r + 10^{x/10})^{2N}}, \qquad x > 0 \quad (18)$$

The mean and the standard deviation of A''_{ij} are

$$\mu_{A''_{ij}} = 10\log_{10}\sigma'_r \quad (19)$$

$$\sigma_{A''_{ij}} = \frac{10\sqrt{2}}{\ln 10}\sqrt{\Psi(1, N)} \quad (20)$$

where $\Psi(k, x) = \mathrm{d}[\ln\Gamma(x)]/\mathrm{d}x$ is the digamma function and

$$\sqrt{\Psi(1, N)} \approx \frac{1}{\sqrt{N}} + \frac{1}{4N^{3/2}} + \frac{5}{96N^{5/2}} + \ldots \quad (21)$$

A plot of $\sigma_{A''_{ij}}$ is given in Figure 2. For the total anisotropy coefficient, the maximum absolute value from the three planar anisotropy coefficients could be used (i.e. $A' \overset{\text{def}}{=} \max(|\mu_{A'_{xy}}|, |\mu_{A'_{xy}}|, |\mu_{A'_{xy}}|)$).

The measurement demonstration is illustrated in Figure 3. In Figure 3(b), a 3-axis E-field probe was used to record the E-fields at 8 probe positions at the corner of the RC working volume, and the stirrer was rotated with 1000 vertical stirrer steps in one revolution. 19 frequency points

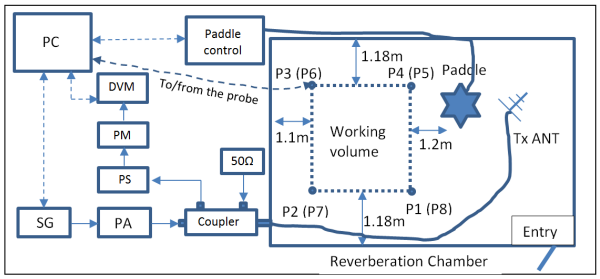

(a)

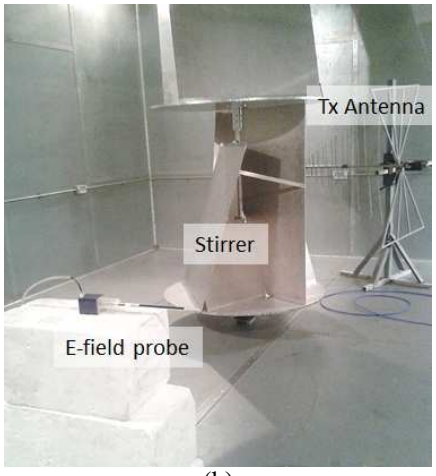

(b)

(c)

Figure 3. (a) Schematic plot of the measurement setup, PC: control computer; SG: signal generator, DVM: digital voltage meter, PS: power sensor, PA: power amplifier, PS: power sensor, (b) measurement scenario in an RC with inner dimensions 6.5 m × 5.9 m × 3.5 m, (c) measurement scenario in an RC with inner dimensions 5.1 m × 3.9 m × 2.95 m.

were measured in the frequency range of 100 MHz – 1 GHz. In Figure 3(c), a vector network analyzer (VNA) was used to record 1001 frequency points from 80 MHz to 1 GHz, and 100 stirrer positions were used for both vertical and horizontal stirrers rotating synchronously.

All the E-fields with the same polarizations from 8 positions are used to calculate A'_{ij}. Note that when a VNA is used, $|S_{21}|^2$ is considered instead of $|E_i|^2$. The measured $\langle A'_{ij} \rangle$ in two RCs with different ij combinations

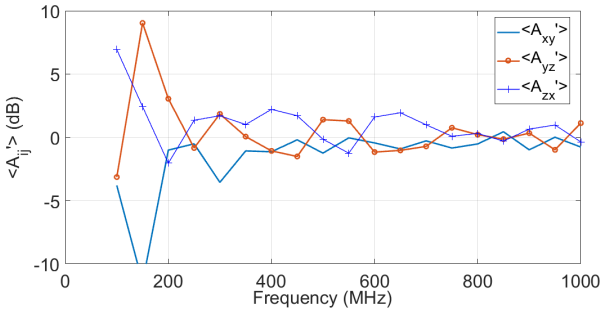

(a)

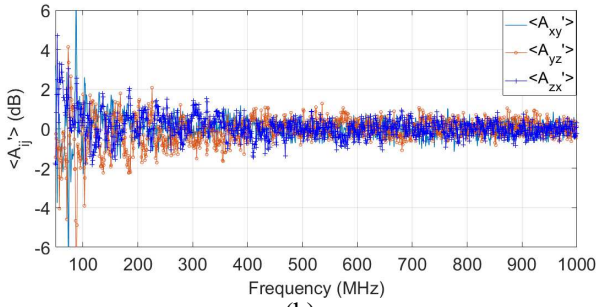

(b)

Figure 4. (a) Measured $\langle A'_{ij} \rangle$ in scenario Figure 3(b), (b) measured $\langle A'_{ij} \rangle$ in scenario Figure 3(c).

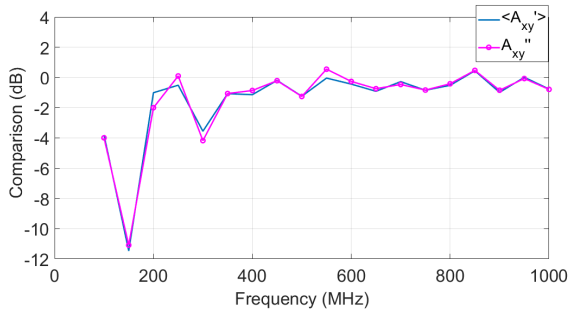

(a)

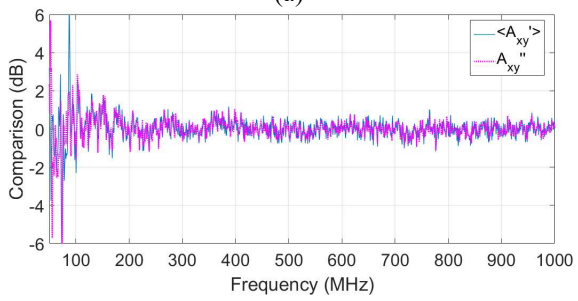

(b)

Figure 5. (a) A comparison of measured $\langle A'_{xy} \rangle$ and A''_{xy} in scenario Figure 3(b), (b) a comparison of measured $\langle A'_{xy} \rangle$ and A''_{xy} in scenario Figure 3(c).

are illustrated in Figure 4(a) and 4(b), respectively. As expected, $\langle A'_{ij} \rangle$ approaches 0 dB towards higher frequencies statistically and the standard deviations become smaller as the independent sample number increases at higher frequencies. Comparisons of typical values of $\langle A'_{ij} \rangle$ and A''_{ij} are illustrated in Figure 5, they give similar values as they have the same mean values in (11) and (19).

TABLE I. A SUMMARY OF ANISOTROPY WITH DIFFERENT DEFINITIONS

Symbol	Definitions	PDF	CDF	Mean	Standard deviation
A_{ij}	$\frac{\lvert E_i\rvert^2 - \lvert E_j\rvert^2}{\lvert E_i\rvert^2 + \lvert E_j\rvert^2}$	$\frac{2\sigma_r}{[\sigma_r + 1 + (\sigma_r - 1)x]}$, $-1 \le x \le 1$	$\frac{(1+x)\sigma_r}{[\sigma_r + 1 + (\sigma_r - 1)x]}$, $-1 \le x \le 1$	$\frac{1 + 2\sigma_r \ln\sigma_r - \sigma_r^2}{(\sigma_r - 1)^2}$	$\frac{2\sqrt{\sigma_r - (2 + \ln^2\sigma_r)\sigma_r^2 + \sigma_r^3}}{(\sigma_r - 1)^2}$
A'_{ij}	$10\log_{10}\frac{\lvert E_i\rvert^2}{\lvert E_j\rvert^2}$	$\frac{10^{\frac{x}{10}-1}\sigma'_r \ln(10)}{(\sigma'_r + 10^{x/10})^2}$, $-\infty \le x \le \infty$	$\frac{10^{x/10}}{\sigma'_r + 10^{x/10}}$, $-\infty \le x \le \infty$	$10\log_{10}\sigma'_r$	$\frac{10\pi}{\sqrt{3}\ln 10}$
A''_{ij}	$10\log_{10}\frac{\langle\lvert E_i\rvert^2\rangle_N}{\langle\lvert E_j\rvert^2\rangle_N}$	$\frac{\Gamma(2N)\ln(10)10^{Nx/10-1}\sigma_r'^N}{\Gamma^2(N)(\sigma'_r + 10^{x/10})^{2N}}$	-	$10\log_{10}\sigma'_r$	$\frac{10\sqrt{2}}{\ln 10}\sqrt{\Psi(1,N)}$

$\sigma'_r = \mu_i/\mu_j = \sigma_r^{-1}$, where μ_i and μ_j are the expected value of $\lvert E_i\rvert^2$ and $\lvert E_j\rvert^2$ respectively.

3. Conclusions

We have proposed alternative definitions to quantify the field anisotropy coefficient in an RC. These alternative definitions could be more direct and intuitive, as the mean value is directly in the form of dB as the ratio of the mean values in different polarizations. Different definitions are summarized in Table I. Mathematically, equivalencies exist between the alternative definitions and the conventional definitions in the IEC 61000-4-21 standard, and they are compatible with each other. Furthermore, validation measurements have also been performed to demonstrate the measured anisotropy coefficients.

4. Acknowledgements

This work was supported in part by the National Natural Science Foundation of China under Grants 61701224, in part by Nanjing Rongce Testing Technology Ltd and in part by the 2021–2025 National Measurement System Programme of the UK Government's Department for Business, Energy and Industrial Strategy, Science Theme Reference EMT22.

References

[1] IEC 61000-4-21, *Electromagnetic compatibility (EMC) – Part 4-21: Testing and measurement techniques – Reverberation chamber test methods*, IEC Standard, Ed 2.0, 2011-01.

[2] L. R. Arnaut, R. Serra and P. D. West, "Statistical anisotropy in imperfect electromagnetic reverberation," *IEEE Transactions on Electromagnetic Compatibility*, vol. 59, no. 1, pp. 3-13, Feb. 2017.

[3] L. R. Arnaut, "Field anisotropy, field inhomogeneity and polarization bias in imperfect reverberation chambers," *Nat. Phys. Lab., Teddington, U.K., Tech. Rep. R981120*, pp. 1–65, Nov. 1998.

[4] L. R. Arnaut, "Operation of electromagnetic reverberation chambers with wave diffractors at relatively low frequencies," *IEEE Transactions on Electromagnetic Compatibility*, vol. 32, no. 4, pp. 637–653, Nov. 2001.

[5] M. Magdowski, E. Suthau, K. Pasche, R. T. Jacobs and R. Vick, "Field homogeneity and isotropy analysis of a reverberation chamber equipped with a pair of hemispherical diffractors," *International Symposium on Electromagnetic Compatibility - EMC EUROPE*, 2020, pp. 1-6.

[6] R. Serra, "Reverberation chambers through the magnifying glass: an overview and classification of performance indicators," *IEEE Electromagnetic Compatibility Magazine*, vol. 6, no. 2, pp. 76-88, 2017.

[7] L. R. Arnaut, R. Serra and P. D. West, "Validating reverberation chamber performance based on assessment of field anisotropy," *International Symposium on Electromagnetic Compatibility - EMC EUROPE*, 2016, pp. 205-210.

[8] L. R. Arnaut, "Elliptic stochastic fields in reverberation chambers," *IEEE Transactions on Electromagnetic Compatibility*, vol. 58, no. 1, pp. 11-21, Feb. 2016.

[9] D. Senic, D. Cavaliere, M. V. Noth, M. G. Becker, K. A. Remley, C.-M. Wang and C. L. Holloway, "Isotropy study for over-the-air measurements in a loaded reverberation chamber," *IEEE International Symposium on Electromagnetic Compatibility & Signal/Power Integrity (EMCSI)*, 2017, pp. 124-129.

[10] N. Wellander, M. Elfsberg, H. Sundberg and T. Hurtig, "Destructive testing of electronic components based on absorption cross section RC measurements," *International Symposium on Electromagnetic Compatibility - EMC EUROPE*, Barcelona, Spain, 2019, pp. 778-783.